

# Traditional CFD Boundary Conditions Applied to Blood Analog Flow Through a Patient-Specific Aortic Coarctation

Xiao Wang<sup>1</sup>, D. Keith Walters<sup>1,2</sup>, Greg W. Burgreen<sup>1</sup>, and David S. Thompson<sup>1,3</sup>

<sup>1</sup> Center for Advanced Vehicular Systems

<sup>2</sup> Department of Mechanical Engineering

<sup>3</sup> Department of Aerospace Engineering

Mississippi State University, Starkville MS 39759, USA

**Abstract.** Flow of a blood analog is modeled through a patient-specific aortic coarctation using ANSYS Fluent software. Details of the patient data (aortic geometry and prescribed flow conditions) were provided by the MICCAI-STACOM CFD Challenge website. The objective is to predict a blood pressure difference across the rigid coarctation under both rest and exercise (stress) conditions. The supplied STL geometry was used to create coarse and fine viscous meshes of 250K and 4.6M cells. Our CFD method employed laminar, Newtonian flow with a total pressure inlet condition and special outlet BCs derived from reconstructed flow waveforms. Analysis setup and outlet BCs were treated as a traditional non-physiological CFD problem. CFD results demonstrate that the supplied AscAo pressure waveform and flow distributions are well matched by our simulations. A non-uniform pressure gradient field is predicted across the coarctation with strong interactions with each supra-aortic vessel branch.

**Keywords:** computational fluid dynamics, aortic arch flow

## 1 Introduction

Physiology of an aorta involves a significant compliant volume change driven by pressure/flow pulses generated by a beating left ventricle. The aorta acts as the central pressurized arterial blood plenum that supplies all major organ systems in the human circulation. CFD analysis of an isolated aorta is challenging because both its dynamic shape and its interaction with the circulation must be realistically approximated. This study performs a highly simplified but physically valid fluid dynamic simulation of an isolated rigid aorta. Directly using the BC data supplied by the website (namely, time-varying pressure/flow profiles at the AscAo and flow profiles at the DescAo), a pressure field is predicted that identically matches the AscAo and DescAo profiles subject to the basic constraint that the three supra-aortic vessels account for the flow differences required to conserve mass. This study intentionally neglects key features defining a physiologically

realistic aorta, particularly, its time varying shape compliance and interaction with fluid dynamically nonlinear vascular subsystems of the circulation. The objective is to generate baseline flow solutions of a simplified idealized aorta for comparisons to physiological data and to other CFD solutions that involve more complex modeling approaches.

## 2 CFD Model Setup

The commercial software package ANSYS Fluent v14.0 was used to perform the simulations. Laminar flow was assumed for the flow throughout the entire cardiac cycle. The working fluid was a Newtonian blood analog with constant density of  $1000 \text{ kg/m}^3$  and viscosity of  $0.004 \text{ kg/ms}$ . The simulations used second-order spatial discretization for the momentum equations, the second order interpolation scheme for discretization of the pressure, and the SIMPLE scheme for pressure-velocity coupling. Unsteady terms were discretized using a second-order implicit scheme.

The time-accurate simulations were based on a repeating cardiac cycle using 400 uniform time steps per cycle. To ensure accuracy of the unsteady solution, 100 subiterations were used at each time step. For each case, unsteady calculations were performed for a time period of two cardiac cycles to ensure that a periodic flow pattern was achieved. Solutions extracted from the second cardiac cycle are reported and analyzed.

At the inlet and outlet boundary surfaces, unsteady flow conditions were incorporated into the FLUENT solver using user-defined function subroutines. The prescribed ascending aortic pressure variation was applied via a spatially uniform, time-varying total pressure boundary condition derived from the supplied waveforms of the ascending aortic pressure and flow rate. A temporally-varying, spatially-uniform velocity boundary condition based on the provided waveform was prescribed at the descending aortic outlet. Flow velocities were also specified at the three supra-aortic vessels (Innominate, LCC, LS). These velocities were based on the instantaneous net flow rate, i.e., the difference between the flow rate entering the domain and the flow rate exiting the domain at the descending aortic outlet. The net flow rate was partitioned among the three outlets to preserve the ratios provided in Table 1. The ratio of flow through each supra-aortic vessel was assumed to be a constant fraction of the total flow through all three vessels. This approach ensures that the correct average flow rate is obtained at each inlet/exit. No-slip conditions were applied at wall boundaries. All walls were considered to be strictly rigid with no fluid-structure interaction.

Volumetric flow rates and spatially-averaged static pressures at each boundary were recorded at every time step to characterize the unsteady flow. In order to evaluate the coarctation pressure gradients consistently with the invasive pressure wire measurements, pressures in the proximal and distal planes at the required locations were recorded at each time step as well.

### 3 Mesh Refinement

A mesh refinement study was performed by comparing results computed on a coarse mesh (250k cells) and a fine mesh (4.57M cells). Both meshes were tetrahedral-dominant with five layers of prismatic boundary layer cells. Simulations were conducted using both meshes under the stress condition. Comparing the time-resolved spatial-average pressure at each boundary surface, slight differences are observed only in the descending pressure data at the descending outlet (Fig. 1(a)). Based on these results the fine mesh was judged to be sufficient for analysis of results.

### 4 CFD Results

The unsteady simulations were conducted for two physiologic states of a patient, in rest condition and in stress condition. The heart rate is 47 beats per minute under rest condition, and 141 beats per minute under stress condition. The corresponding cardiac cycle is 1.277 seconds for rest condition, and 0.45 seconds for stress condition.

#### 4.1 Rest Condition

For the rest condition, unsteady simulations were performed for a time period of two cardiac cycles (cardiac cycle 1.277 sec, total flow time 2.554 sec) using total 800 time steps with a uniform step size of  $3.1925e-3$  sec.

Fig. 1(b) shows that the static pressure obtained at the ascending boundary in the CFD simulations and the supplied ascending aortic pressure are in good agreement, which indicates that the total pressure specified at the inlet face matches the given inlet condition. The unsteady flow rate at the ascending inlet should automatically match the supplied ascending aortic flow waveforms when all the outlet boundary flow rates are specified based on the given flow conditions. Fig. 1(c) depicts the time history of predicated pressure gradients responding to the flow waveforms. Solutions of pressure and velocity fields were extracted at the instant of peak flow (0.19 sec) as shown in Figs. 2, 3 and 4.

The aorta wall pressure shown in (Fig. 2) indicates that the pressure distribution in the supra-aortic vessels are related to their size. The left carotid artery (LCC) is the narrowest branch with lower flow rate and lower pressure. A cutting plane shown in Fig. 3 details the pressure change in the aorta interior. The higher ascending pressure pumps blood into the supra-aortic vessels. As the flow of blood is turning at the arch of aorta, pressure drops quickly until it enters the descending aorta, thereafter flow pressure is gradually decreasing to reach the lowest value at the descending outlet.

Contours of flow velocity magnitude in Fig. 4 reveal two regions of flow separation. The arch of the aorta induced large flow separations due to the sudden change of flow direction. Another thin layer of separation is observed on the wall of the descending aorta. The coarctation (i.e. narrowing or pinching) in

the aorta of this patient, between the aortic arch and descending aorta, forms a shape similar to a converging-diverging nozzle. The diverging wall produces adverse pressure gradients on the boundary layer, and encourages flow separation, which helps to explain the separations that occur on the diverging section of the aorta wall.

## 4.2 Stress Condition

For the stress condition, unsteady simulations were also performed for a time period of two cardiac cycles (cardiac cycle 0.425 sec, total flow time 0.85 sec) using a total of 800 time steps with a uniform time step of  $1.0625 \times 10^{-3}$  sec. The predicted pressure gradient corresponding to the supplied flow rate is presented in Fig. 1(d).

For the stress condition, all of the outlet branches experienced large pressure drops at peak flow (Fig. 2) indicating higher cardiac workload on all the supra-aortic vessels.

For the stress condition, the lowest pressure appears at the aortic arch, rather than the descending outlet as in the rest condition case (compared in Figs. 2 and 3). Flow separations also occur in the region around the arch and on the diverging wall downstream the site of the coarctation in the descending aorta (Fig. 4). However, due to the higher flow velocity under stress condition, the separated boundary layer grows along one side of the descending aorta wall. On the other side of the wall, flow retains higher velocity and no separation is observed.

Tables 1 and 2 summarize the average values of flow rates and pressures over one cardiac cycle. Throughout the cardiac cycle, the flow splitting ratios among the three supra-aortic vessels were assumed constant and estimated by the supplied average flow rates through each upper branch. Considering the fact that this simple boundary condition of constant flow ratio is not physiologically accurate, the effect of flow splits on the coarctation pressure gradients was further investigated.

## 4.3 Effect of flow splits on pressure prediction

At any given instant of time, specific flow splits into the innominate, left carotid, and left subclavian arteries remain unknown. It should be noted that, other than non-uniformity of flow variables at inlets and outlets, this was the only remaining degree of freedom provided by the problem constraints. Since pressure gradients are highly dependent on the supra-aortic flow rates, the effects of different supra-aortic flow splits on predicted pressure gradients in the aorta were investigated. To this end, two additional simulations were performed for the stress condition on the coarse mesh, namely, a condition that assumed supra-aortic flow evenly split among the three upper branches; and a condition that arbitrarily assumed all supra-aortic flow is shunted only through the left carotid artery with the other two branches 100% blocked.

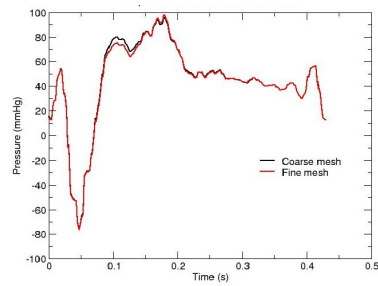
Fig. 5 shows the predicted pressure gradients corresponding to the supplied flow waveforms with different supra-aortic flow splits. The proximal plane is located upstream of the upper branches and close to the ascending inlet where the supplied pressure waveform is imposed. Hence, the predicted pressure at the proximal plane is little affected by the flow splitting at the upper branches. However, for distal locations at the arch and beyond, the effects of the different flow splitting ratios are stronger as evidenced by the larger pressure differences during the instances of peak flow. At lower flow rates, the splitting influences are limited. Overall, the influence of flow splitting on pressure gradients over time is moderate as indicated by the small differences in time-averaged mean values summarized in Table 2.

## 5 Conclusions

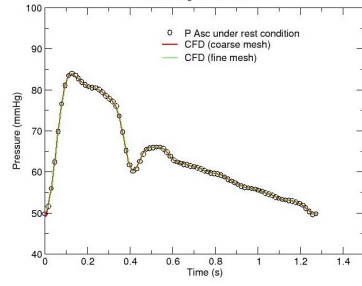
Unsteady flow simulations of a patient-specific aortic coarctation were conducted based on the supplied flow conditions using ANSYS Fluent software. For simplification purposes, laminar Newtonian flow, rigid aortic walls, and traditional CFD outlet BCs were assumed. Physiology-based boundary conditions and fluid-structure interactions were not considered, which challenges the accuracy of the present results. At the end of the 4<sup>th</sup> International Workshop STACOM 2013, the measured pressure gradients were released. Compared to the measured pressure gradients (shown in Table 2), peak pressure gradients are dramatically overestimated in current work. Future studies need to systematically identify and correct deficiencies of the present simplified CFD approach.

**Table 1.** CFD-predicted total flow rates (L/min) through outlets

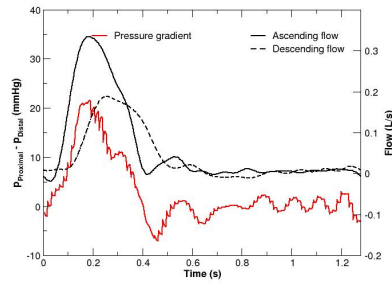
Outlet	Rest Condition			Stress Condition		
	Supplied	CFD		Supplied	CFD	
		Fine Mesh	Coarse Mesh		Fine Mesh	Coarse Mesh
AscAo	3.71	3.73	3.70	15.53	13.64	13.54
Innominate	0.624	0.630	0.625	3.355	3.384	3.358
LCC	0.312	0.306	0.294	0.6875	0.6989	0.6716
LS	0.364	0.372	0.368	1.4575	1.4950	1.4775
DiaphAo	2.41	2.42	2.41	8.03	8.06	8.04



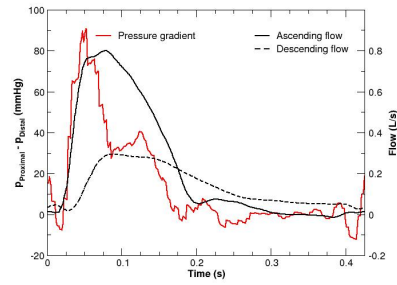
(a)



(b)



(c)



(d)

**Fig. 1.** (a) Static pressure at descending outlet shows only slight differences between coarse and fine mesh. (b) Static pressure at ascending inlet under rest condition. (c) Pressure gradient and flow waveforms under rest condition. (d) Pressure gradient and flow waveforms under stress condition.

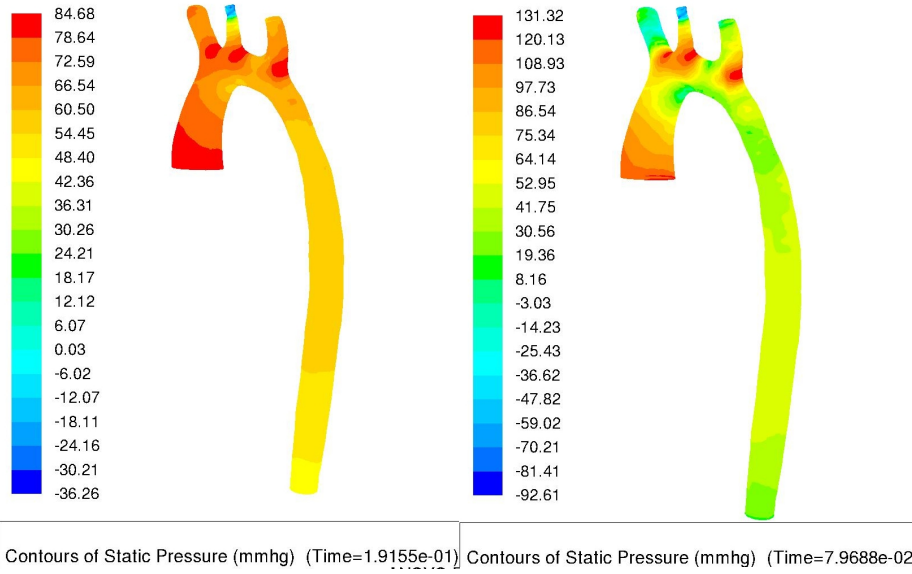


**Fig. 2.** Aorta wall pressure at the instant of peak ascending flow at rest (left) and stress (right) condition.

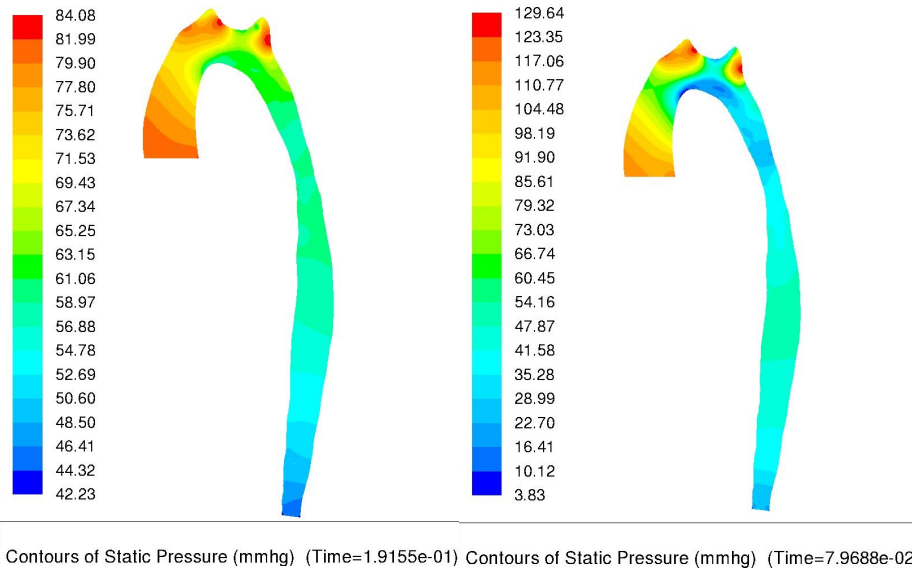


**Fig. 3.** Pressure in aorta cutting plane at the instant of peak ascending flow at rest (left) and stress (right) condition.

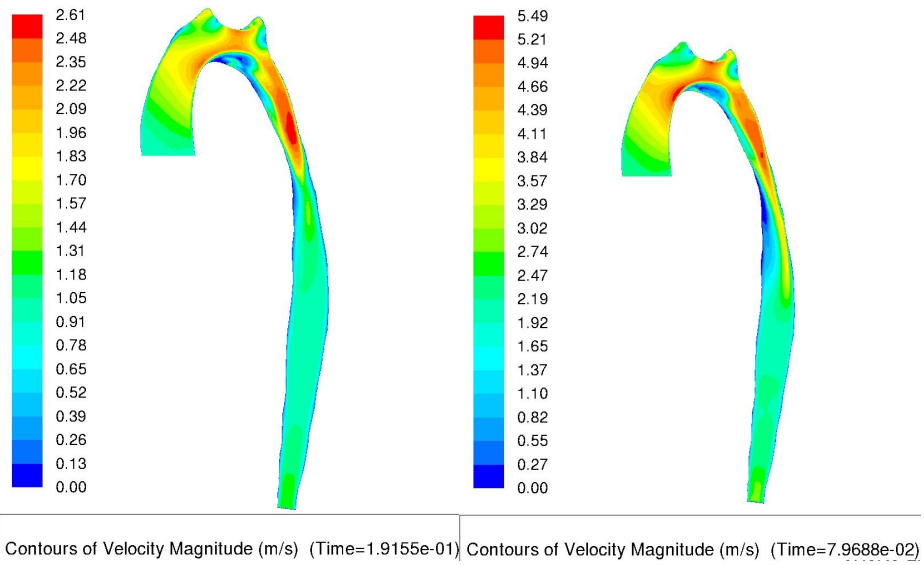


**Fig. 4.** Velocity magnitude in aorta cutting plane at the instant of peak ascending flow at rest (left) and stress (right) condition.

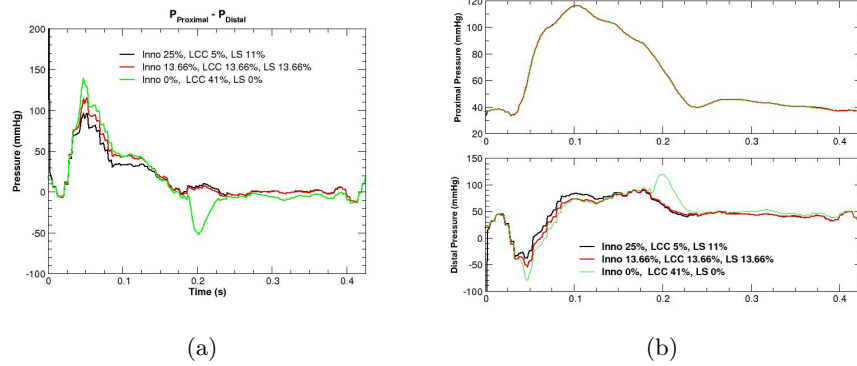


**Fig. 5.** (a) Pressure gradient variation with different supra-aortic flow splits. (b) Pressure (mmHg) at proximal and distal locations.

**Table 2.** CFD-predicted pressure gradients (mmHg):  $dp = P_{Proximal} - P_{Distal}$

		Rest			Stress		
		Min.	Max.	Mean	Min.	Max.	Mean
$P_{Proximal}$	Fine mesh	49	81	63	29	111	60
$P_{Distal}$	Fine mesh	48	73	60	-38	89	47
$dp$	Fine mesh	-7	21	2.8	-12	90	14
	measured (released at STACOM13)		6.50	1.23		45.74	14.65
$dp$	flow split test cases on coarse mesh						
	Inno 25%,LCC 5%, LS 11% of AscAo				-12	96	15
	evenly split				-12	115	17
	through LCC only				-12	138	13